

Deformation capacity of thin reinforced concrete shear walls

C.L. Segura & J.W. Wallace

Department of Civil Engineering, University of California, Los Angeles, United States.

C.A. Arteta

Department of Civil and Environmental Engineering, Universidad del Norte, Barranquilla, Colombia.

J.P. Moehle

Department of Civil Engineering, University of California, Berkeley, United States.



2016 NZSEE
Conference

ABSTRACT: The extent of damage observed near the base of shear walls of reinforced concrete buildings following earthquakes in Chile in 2010 and New Zealand in 2011 exceeded expectations of the engineering community. Brittle flexure-compression failures and lateral (out-of-plane) instability of compression zones in modern walls implies deficiencies in design standards and a need to better understand the failure mechanisms that may develop in flexure-dominant walls. Experimental results of the compressive strain capacity of a reinforced concrete prism specimen, representative of the boundary element of a special structural wall (ACI 318 designation), are presented. A relationship between usable compressive strain limits and the height over which plastic deformations spread is provided. The results of a complementary shear wall panel test, designed with a boundary region matching the geometry and reinforcement arrangement of the prism specimen, are also presented. Comparisons are made between usable strain limits of the uniformly compressed prism specimen and the boundary element compressive strains of the wall specimen for which a strain gradient exists at the boundary under combined axial load and overturning. These tests provide crucial information about the impact of boundary element compressive strains on wall global deformation capacities (drift).

1 INTRODUCTION

Damage localization at the base of several multi-story reinforced concrete wall buildings was reported following earthquakes in Chile and New Zealand (Alarcon et al. 2015; Wallace et al. 2012; Westenenk et al. 2013; Kam et al. 2011). It is hypothesized that these failures were non-ductile based on observations of damage concentration over a short height, crushing of concrete, buckling of longitudinal reinforcement, fracture of confining hoops and cross-ties, opening of cross-tie hooks, and out-of-plane instability of wall compression zones. In some cases, poor confinement, high slenderness of compression zones, and large axial stress ratios are suspected to have contributed to poor performance (Wallace 2012; Massone et al. 2012); however, observed flexure-compression failures in tension-controlled walls satisfying modern design codes suggests shortcomings in the design process that need to be addressed.

Changes have been incorporated into ACI 318-14 to address some of these issues; however, insufficient information existed to develop code change proposals to address some potential concerns. The experimental program described herein was a joint effort between researchers at the University of California, Berkeley and at the University of California, Los Angeles. The primary goals were to characterize the deformation capacity of thin walls controlled by flexure-compression actions, and to identify critical detailing issues. Full-scale rectangular prismatic specimens, representative of the boundary element of a special structural wall (ACI 318 designation), were tested under uniform compression until failure. Complementary tests on wall panel specimens were conducted to

understand the deformation capacity of critical regions of relatively thin special structural walls. Results are presented for representative tests of one boundary element prism and one wall panel.

The need for special boundary element (SBE) detailing at the edges of structural walls is evaluated according to ACI 318 using either a stress-based or a displacement based approach. By the stress-based approach, SBE detailing is required at wall edges if the extreme fiber compressive stress demand, due to axial load and overturning, exceeds 20% of the nominal compressive strength of the concrete (i.e., $\sigma_u \geq 0.2f'_c$). The compressive stress demand is estimated by means of a linear elastic model, using load combinations that include earthquake effects and using gross concrete cross section properties. The displacement-based approach applies to walls that are effectively continuous from the base of the structure to the top of the wall, designed to have single critical section for flexure and axial load. SBE detailing is required at wall edges by the displacement-based approach if:

$$c \geq \frac{l_w}{600[\gamma(\delta_u/h_w)]} \quad (1)$$

where c corresponds to the largest neutral axis depth calculated for the factored axial force and nominal moment strength in the direction of the design displacement δ_u ; coefficient γ is 1.0 in ACI-318-11 and 1.5 in ACI-318-14; l_w and h_w are the length and height of the wall, respectively.

Where SBEs are required, the quantity of transverse reinforcement provided must comply with **Equation 3** per ACI-318-11, and **Equations 2** and **3** per ACI-318-14:

$$\frac{A_{sh}}{sb_c} \geq 0.3 \frac{f'_c}{f_{yt}} \left(\frac{A_g}{A_{ch}} - 1 \right) \quad (2)$$

$$\frac{A_{sh}}{sb_c} \geq 0.09 \frac{f'_c}{f_{yt}} \quad (3)$$

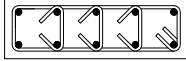
where s is the center-to-center spacing of transverse reinforcement; b_c is the cross-sectional dimension of the core measured to the outside edges of the transverse reinforcement; A_{sh} is the total quantity of transverse reinforcement provided within spacing s and perpendicular to dimension b_c ; A_g is the gross area of the concrete section; A_{ch} is the cross-sectional area of the core measured to the outside edge of the perimeter hoop; f'_c is the specified unconfined concrete compressive strength; and f_{yt} is the specified yield strength of the transverse reinforcement.

Where SBEs are not required, ACI 318-11 limits transverse reinforcement spacing to 8 in. [20 cm] if the boundary element longitudinal reinforcement ratio exceeds $400/f_y$, where f_y is the specified yield strength of the boundary longitudinal reinforcement. Additional provisions were incorporated into ACI 318-14, limiting transverse reinforcement to the smaller of 8 in. [20 cm] and 8 bar diameters (d_b), except at yielding sections, where spacing of transverse reinforcement is limited to the smaller of 6 in. [15 cm] and $6d_b$.

2 TEST ON A FULL-SCALE RECTANGULAR PRISM

A full-scale reinforced concrete prismatic specimen, denoted W12, was designed and constructed in accordance with ACI 318-11 provisions for SBEs, and satisfied the more stringent provisions of ACI 318-14. The specimen was representative of the boundary element at the edge of the critical section of a multi-story shear wall. The reinforcing cage is presented in **Figure 1a**. Global dimension of the portion under consideration were: width = 36 in. [914 mm]; height = 72 in. [1829 mm]; and thickness = 12 in. [305 mm]. This volume was bounded by two loading heads of larger cross-sectional area. Cover thickness to the outer edge of the perimeter hoop was set to 1.5 in. [38 mm]. Design nominal concrete strength was $f'_c = 4.0$ ksi [28 MPa] at 28 days and reinforcing steel yield strength was $f_y = 60.0$ ksi [414 MPa]. All reinforcing steel was compliant with standard ASTM-A706/A706M-9b (2009). **Figure 2** depicts the variables describing the longitudinal and transverse reinforcement layout within the cross section. As-tested concrete and steel material properties along with the geometry of the reinforcement layout are summarized in **Table 1**.

Table 1. As tested material properties and reinforcement detailing.

ID	Cross section	f'_c	f_y	f_{yt}	d_b	ρ_l	s	s/d_b	h'_x	d_{bt}	ρ_x	ρ_y	$\rho_{l,ACII}$	$\rho_{l,ACI2}$
		ksi (MPa)	ksi (MPa)	ksi (MPa)	in. (mm)	%	in. (mm)		in. (mm)	in. (mm)	%	%	%	%
W12		4.4 (30)	77.6 (535)	70.3 (485)	1 1/4 (32)	2.9	4.0 (102)	3.2	7.7 (196)	5/8 (16)	1.70	1.16	0.85	0.56

f_{yt} : transverse steel yield strength; d_b : longitudinal bar diameter; ρ_l : longitudinal steel ratio (area of longitudinal steel divided by gross cross-sectional area); s : transverse reinforcement spacing; A_{shx} : total cross-sectional area of transverse reinforcement within spacing s , in the long direction of the section; A_{shy} : total cross-sectional area of transverse reinforcement within spacing s , in the short direction of the section; b_{c1} : dimension of the long direction of the section core; b_{c2} : dimension of the short direction of the section core.
 $\rho_x = A_{shx}/(b_{c2}s)$ and $\rho_y = A_{shy}/(b_{c1}s)$ are the provided transverse reinforcement ratios in the two principal directions of the cross section; $\rho_{l,ACII} = 0.3f'_c/f_{yt} (A_g/A_{ch} - 1)$ and $\rho_{l,ACI2} = 0.09f'_c/f_{yt}$ are estimated using “as tested” materials properties.

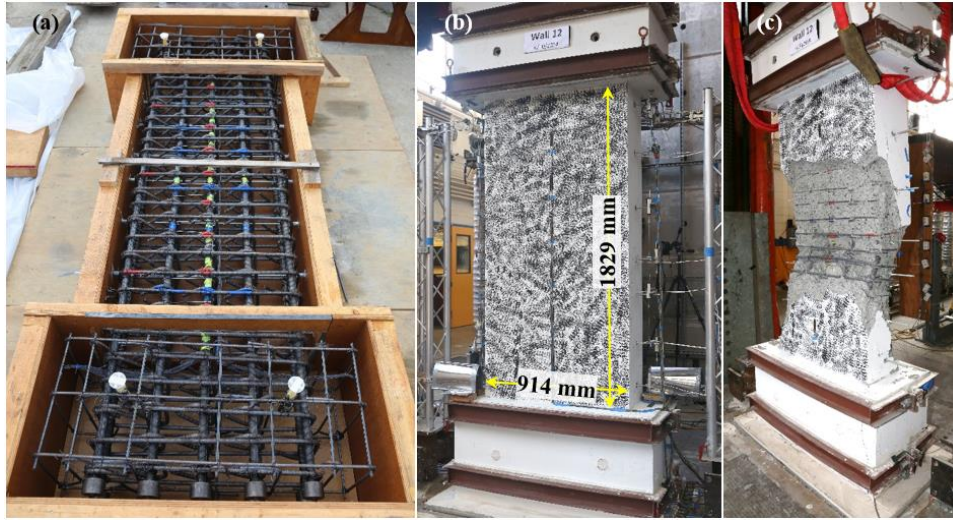


Figure 1. Specimen W12: (a) reinforcing steel cage; (b) test setup; (c) after-the-test

2.1 Test setup

The specimen was tested in the 4-million-pound universal testing machine at the *nees@berkeley* laboratory. **Figure 2** shows the location of two types of concrete strain gages to measure axial (vertical) strains at six discrete locations along the height of the specimen: one set (Co_{SG}) comprises ceramic strain gages embedded in the centroid of the cross section, and another set (Co_{vSG}) comprises wire strain gages adhered to the surface of the concrete cover.

2.2 Test results

The specimen was tested under monotonic uniform compressive loading until failure. **Figure 3a** presents the force versus average strain measured over the 72 in. [1829 mm] height between the loading heads (grey curves). The maximum load carrying capacity of the specimen was limited by the onset of concrete cover spalling, demarcating a softening post-peak response. The asymmetric nature of the cover spalling process introduced an out-of-plane moment that induced additional compressive stresses on the face where spalling initiated. The specimen failed due to out-of-plane lateral instability at an average axial strain of approximately 1.8%. **Figures 1c** and **3b** show the appearance of the specimen after the test was concluded. The out-of-plane instability is apparent. Contrary to observations in other specimens of the same experimental campaign (Arteta et al. 2014), bar buckling of specimen W12 was prevented due to the small ratio between the transverse reinforcement spacing and the longitudinal bar diameter ($s/d_b = 3.2$), but also because hook opening of the reinforcing ties was inhibited due to the large diameter transverse reinforcement ($d_{bt} = 5/8$ in. [16 mm]).

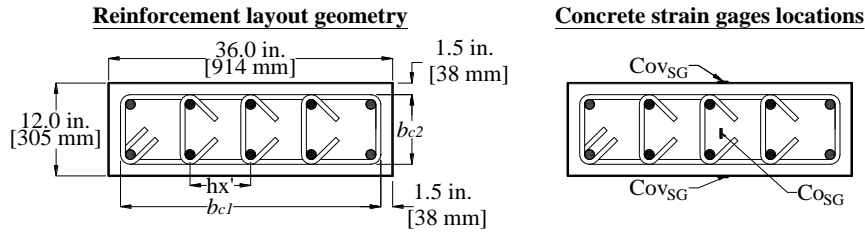


Figure 2. Reinforcement layout and location in plan of core and cover strain gages

Figure 3 summarizes test results recorded by concrete strain gages, along with a view of the most damaged zone on the West face of the specimen (**Figure 3b**). **Figure 3a** presents normalized-force versus pointwise axial strain measurements of the core (using the CO_{SG} set). **Figure 3c** shows the maximum strain attained by the concrete cover (CO_{vSG}) at the same locations on the West face. Onset of concrete cover spalling initiated in portions closest to Lev 3, which coincides with a concentration of axial compressive strain demand in the CO_{SG} of the same location. Relaxation of adjacent CO_{SG} is apparent and indicative of demand concentration over a portion of approximately 2.5 times the specimen thickness ($2.5t_w$).

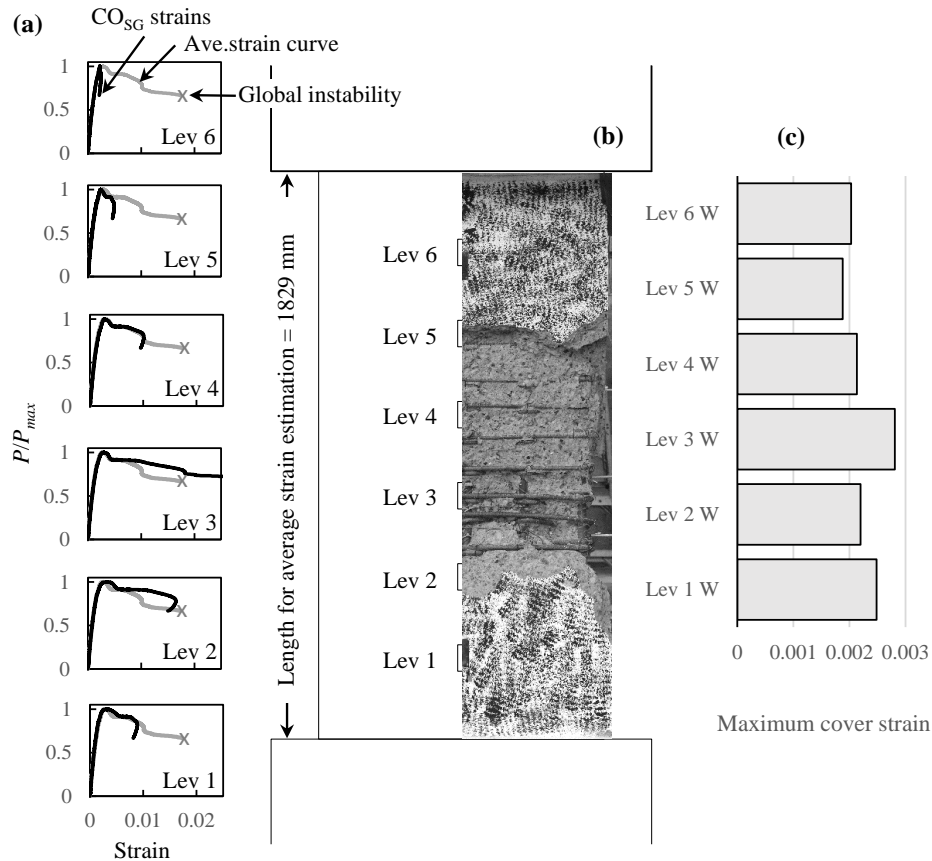


Figure 3. Discrete location in elevation of core and cover strain gages, comparison of local (CO_{SG}) and average strains along the height, and maximum strains attained by the West face concrete cover of specimen W12.

The softening nature of the response of specimen W12 indicates that the post peak demand is concentrated over a relatively short height of the specimen, accompanied by relaxation in adjacent regions. With the aim of estimating usable strain limits for different gage lengths, the strain capacity for several strength levels is defined as follows: ϵ_{100} is the strain at which the maximum load is attained, and ϵ_{90} and ϵ_{80} are the strain measurements at which the maximum load has dropped 10% and 20%, respectively. Strength losses beyond the aforementioned limits are not considered. **Figure 4** shows usable strain for three gage lengths which are estimated by averaging the strain recorded by

one, two, and three adjacent CO_{SG} to that in Lev 3. The strain capacity decreases for increasing values of gage length. For the case where the strains are estimated over $2.2t_w$, the usable compressive strain values ϵ_{100} , ϵ_{90} and ϵ_{80} are 0.3%, 1.0%, and 1.3%, respectively.

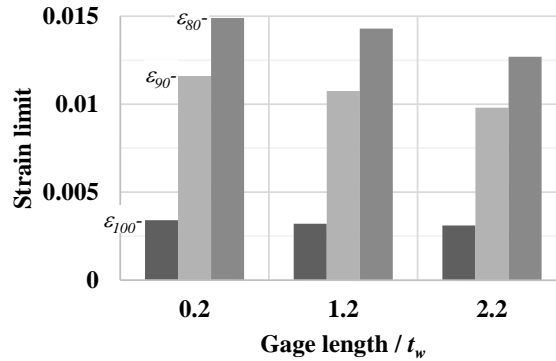


Figure 4. Usable compressive strain for various gage lengths normalized by the specimen thickness.

3 SHEAR WALL PANEL TEST

A half-scale reinforced concrete wall panel specimen, denoted WP4, was constructed and tested at the University of California, Los Angeles Structural/Earthquake Engineering Laboratory. The wall panel was representative of the lower portion of a ten story cantilever wall designed for a single critical section for flexure and axial load. The specimen was tested under combined axial load and reversed cyclic moment and shear. Axial load was held constant throughout the test at $0.10A_w f'_c$. Design nominal concrete compressive strength was $f'_c = 5.0$ ksi [35 MPa] and reinforcing steel yield strength was $f_y = 60$ ksi [414 MPa].

The specimen had a T-shape cross-section (**Figure 5a**) with an enlarged boundary region (flange) at one end of the wall. Boundary longitudinal reinforcement consisted of ten 16 mm diameter bars ($A_b=198mm^2$, $A_s=1980mm^2$) at the web boundary and fourteen 19 mm diameter bars ($A_b=285mm^2$, $A_s=3990mm^2$) at the flange boundary. Web longitudinal and transverse reinforcement consisted of two curtains of 9.5 mm diameter bars ($A_b=71mm^2$) spaced at 20 cm on center ($\rho=0.0046$). Compression depth for an extreme fiber compressive strain of 0.003 was $0.30l_w$ and $0.08l_w$ for compressive stress applied to the web boundary and flange boundary, respectively. The displacement-based design approach of ACI 318-14 was used to determine the need for SBE detailing at each end of the wall. For typical design drift values (i.e., 1%-2%), SBE detailing would be required for the web boundary; thus, boundary transverse reinforcement was selected to satisfy **Equations 2 and 3**. Boundary transverse reinforcement consisted of 8.1 mm diameter ($A_b=52mm^2$) hoops and cross-ties spaced at 51 mm on center ($s/d_b=3.2$). As such, the web boundary element geometry and reinforcement was a half-scale representation of the W12 prismatic specimen. For the short compression depth on the flange boundary, SBE detailing would not be required for typical design drift values. ACI 318-14 provisions for non-special detailing were used at the flange boundary and transverse reinforcement consisted of two 6.4 mm diameter hoops ($A_b=32mm^2$) spaced at 114 mm on center ($s/d_b=6.0$).

3.1 Test setup

The test setup is shown in **Figure 5b**. Increasing cyclic wall rotations were imposed using two vertically-aligned actuators and one horizontally-aligned actuator. Two vertical control sensors positioned at opposite ends of the wall were used to compute wall rotations over an assumed plastic hinge length of one-half the length of the wall. The applied loading pattern simulated the axial load, shear force, and overturning moment demand expected in the lower portion of a ten story cantilever wall. Axial load was applied using two hydraulic jacks mounted above an axial load transfer beam and attached to high-strength post-tensioning rods anchored to the laboratory strong floor. An out-of-plane restraint system was attached to the load transfer beam to prevent out-of-plane movement of the specimen top cap. Columns of vertically-mounted mounted linear variable differential transducers

(LVDTs) were attached to the faces of the specimen to measure wall axial (flexural) deformations at various locations along the length of the wall.

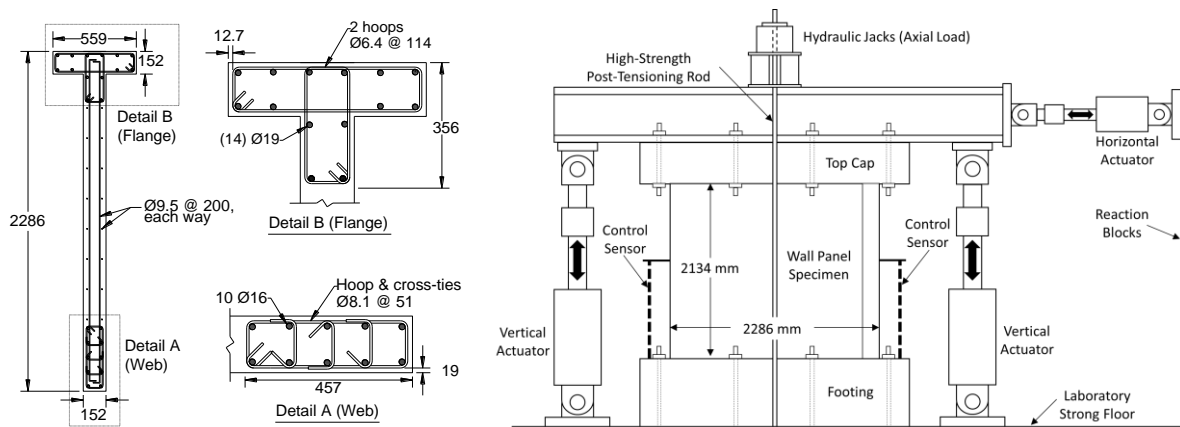


Figure 5. Specimen WP4: (a) Cross-section; (b) Test setup.

3.2 Test Results

The experimentally measured base overturning moment vs. hinge rotation result is presented in **Figure 6**. At approximately 0.75% rotation, vertical splitting and minor crushing of concrete was observed on the edge of the wall at the web boundary. Peak capacity occurred at approximately 0.91% rotation, followed by minor crushing along the front and rear faces of the specimen. At approximately 1.32% hinge rotation, abrupt crushing at the web boundary occurred. Damage extended horizontally from the edge of the wall a distance of nearly two-thirds the wall length, and included crushing of the wall web and buckling of ten web longitudinal bars. Damage to the wall immediately following the crushing failure is shown in **Figure 7b**. Prior to the failure, no visible signs of lateral (out-of-plane) deformation were evident; however, as crushing occurred, the compression zone deformed out-of-plane.

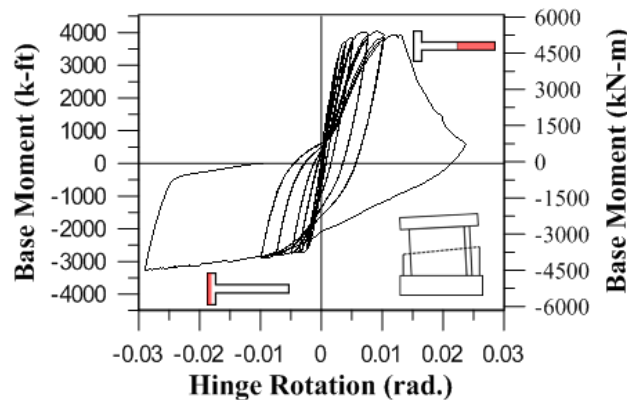


Figure 6. Experimentally measured base rotation vs. hinge rotation.

Backbone curves for the average extreme fiber compressive strain measured at three different heights on the specimen are presented in **Figure 7a** for loading causing compression at the web boundary. The strains were measured by LVDTs attached to the rear face of the specimen, indicated as Sensor 1 in **Figure 7c**. The three levels over which strains were measured are: Lev1) the bottom 14 in. [356 mm] (equal to approximately $2.3t_w$) where crushing of the confined boundary and web occurred, Lev2) between 14 in. and 26 in. [356 mm - 660 mm] above the specimen footing, just above the damaged region, and Lev3) between 26 in. and 44 in. [660 mm - 1118 mm] above the specimen footing. For each level, the average strain measured over an assumed hinge length of $L_w/2$ is also presented as a grey line. Markers are provided on each figure to indicate the corresponding wall hinge rotation at 0.5%, 0.75%, and 1.0% rotation. For loading beyond approximately 0.75% rotation, strains concentrated within the bottom $2.3t_w$, and relaxation of strains occurred at the levels directly above.

Figure 7c displays the average strains measured by two sensors within the bottom $2.3t_w$ of the wall, and demonstrates the influence of a strain gradient. Sensor 1 was located near the edge of the wall, and the strains measured by this sensor match those presented in **Figure 6b** Lev1 (i.e., Sensor 1 represents extreme fiber strain). Sensor 2 was located near the inner edge of the boundary region, at a distance of $0.16l_w$ from the edge of the wall. As previously indicated, compression depth for an extreme fiber compressive strain of 0.003 was $0.30l_w$; thus, strains measured by Sensor 2 are expected to represent the average strain on the compression zone. The measured strain at peak load capacity was 0.9% for Sensor 1 and 0.5% for Sensor 2. Just prior to crushing of the boundary region, at approximately 95% of peak load capacity, the measured strain was 2.3% for Sensor 1 and 1.0% for Sensor 2. A comparison to **Figure 4**, demonstrates good correlation between Sensor 2 results and usable strains from the uniform compression test, for a gage length of $2.2t_w$.

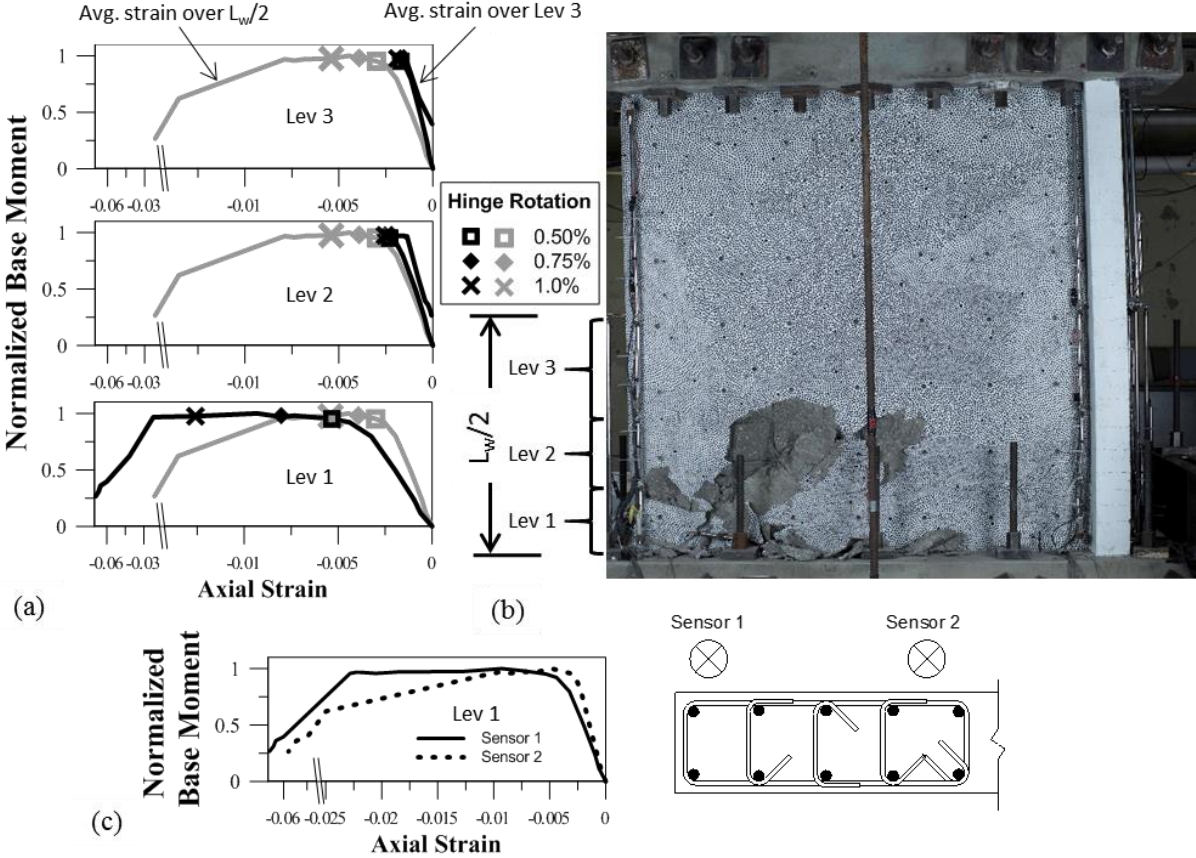


Figure 7. Average compressive strain measured over discrete LVDT sensor heights

4 CONCLUSIONS

Experimental results of the compressive strain capacity of a boundary element prism specimen and the compression region of a wall panel specimen were presented. The boundary element specimen was representative of the compression region of a thin reinforced concrete wall, and satisfied ACI 318-11 and ACI 318-14 provisions for special boundary element detailing. The wall panel specimen was constructed with a boundary region matching the geometry and reinforcement arrangement of the boundary element specimen. Experimental results of the uniform compression test demonstrated that plasticity concentrates over a short height following crushing of cover concrete in thin compression members. Significant strain capacity was achieved within the critical section as relaxation of strains occurred at adjacent heights. Similar behaviour was observed at the boundary of the wall panel following crushing and spalling of concrete cover at the edge of the wall. Good correlation was observed between the usable strains measured from the uniform compression test and the strains measured near the center of the compression zone in the wall panel specimen.

5 REFERENCES

- ACI-Committee-318. (2011). Building Code Requirements for Structural Concrete and Commentary (ACI 318-11). Farmington Hills, MI: American Concrete Institute.
- ACI-Committee-318. (2014). Building Code Requirements for Structural Concrete and Commentary (ACI 318-14). Farmington Hills, MI: American Concrete Institute.
- Arteta C.A., To, D.V. & Moehle, J.P. 2014. Experimental response of boundary elements of code-compliant reinforced concrete shear walls, *Proceedings of the 10th National Conference on Earthquake Engineering, Anchorage, July 21-25 2014*.
- ASTM-A706/A706M-9b. 2009. Standard Specification for Low-Alloy Steel Deformed and Plain Bars for Concrete Reinforcement (pp. 6). West Conshohocken, PA: ASTM International.
- Alarcón, C., Hube, M.A., Jünemann, R. and de la Llera, J.C., 2015. Characteristics and displacement capacity of reinforced concrete walls in damaged buildings during 2010 Chile earthquake, *Bulletin of Earthquake Engineering*, Vol 13(4) 1119-1139.
- Kam, W.Y., Pampanin, S., & Elwood, K. 2011. Performance of concrete buildings in the 22 February Christchurch (Lyttelton) earthquake, *Bulletin of the New Zealand Society for Earthquake Engineering*, 44(4) 239-278.
- Massone, L. M., Bonelli, P., Lagos, R., Luders, C., Moehle, J. P., & Wallace, J. W. 2012. Seismic design and construction practices for RC structural wall buildings, *Earthquake Spectra*, Vol 28(S1) S245-S256.
- Wallace, J. W. 2012. Behavior, design, and modeling of structural walls and coupling beams – Lessons from recent laboratory tests and earthquakes, *International Journal of Concrete Structures and Materials*, Vol 6(1) 3-18.
- Wallace, J. W., Massone, L. M., Bonelli, P., Dragovich, J., Lagos, R., Luders, C., & Moehle, J. P. 2012. Damage and Implications for Seismic Design of RC Structural Wall Buildings, *Earthquake Spectra*, Vol 28(S1) S281-S299.
- Westenenk, B., de la Llera, J.C., Jünemann, R., Hube, M.A., Besa, J.J., Lüders, C., Inaudi, J.A., Riddell, R., Jordán, R. 2013. Analysis and interpretation of the seismic response of RC buildings in Concepción during the February 27, 2010, Chile Earthquake, *Bulletin of Earthquake Engineering*, Vol 11(1) 69–91.